Proceedings of ASME Turbo Expo 2011
GT2011
June 6-10, 2011, Vancouver, British Columbia, Canada

GT2011-46729

AN INVERSE DESIGN BASED METHODOLOGY FOR RAPID 3D MULTI-OBJECTIVE/MULTIDISCIPLINARY OPTIMIZATION OF AXIAL TURBINES.

Pietro Boselli and Mehrdad Zangeneh
Department of Mechanical Engineering
University College London
London WC1E 7JE

ABSTRACT

Design of axial turbines, especially LP turbines, poses difficult tradeoffs between requirements of aerodynamic design and structural limitations. In this paper, a methodology is proposed for 3D multi-objective design of axial turbine blades in which a 3D inverse design method is coupled with a multi-objective genetic algorithm. By parameterizing the blade using blade loading parameters, spanwise work distribution and maximum thickness, a large part of the design space can be explored with very few design parameters. Furthermore, the inverse method not only computes the blade shape but also provides accurate 3D inviscid flow information. In the simple multi-disciplinary approach proposed here the different losses in axial turbines such as endwall losses, tip leakage losses and an indication of flow separation are related through well known correlations to the blade surface velocities predicted by the inverse design method. In addition, geometrical features such as throat area, lean angles and airfoil cross sectional area are computed from the blade shape employed during the optimization. Also, centrifugal stresses and bending stresses are related to the blade geometry. The methodology is then applied to the redesign of an LP turbine rotor with the aim of reducing the maximum stresses while maintaining the performance of the rotor. The results are confirmed by using the commercial CFX CFD (Computational Fluid Dynamics) code and Ansys FEA (Finite Element Analysis) codes.

NOMENCLATURE

a_2	Outlet flow angle
c	Blade chord
C_d	Discharge coefficient
C_{dis}	Entropy dissipation coefficient
$\partial/\partial m$	Meridional derivative
E	Young's Modulus
g	Blade tip gap
h	Blade height
p	Blade pitch
r	Radius (radial co-ordinate)
σ_y	Yield Stress
V_2	Outlet fluid velocity
V_p	Pressure surface velocity
V_s	Suction surface velocity
$\bar{V}_\theta$	Mean tangential velocity
w	Local suction to pressure surface gap
T	Stagnation temperature

INTRODUCTION

Design of turbomachinery blades is increasingly subject to a broad range of multi-objective requirements in terms of aerodynamic performance and structural integrity. The iterative process between the aerodynamic and structural design creates major bottlenecks in design. Automatic optimization can play a major part in the design process to reduce development time and to explore the design space in a more systematic manner.

Development of any optimization technique is dependent on three major building blocks: the geometry parameterization, the performance parameter evaluator and the optimization algorithm.

A good geometry parameterization has to represent the largest possible design space with the fewest parameters. The blade shape is usually parameterized through direct geometrical representation, most notably stacked simple B-spline profiles [1-2-3-4-5], NURBS surfaces [6,7], and quasi 3D sections defined through Bezier curves [8]. In order to reduce computational complexity or avoid unfeasible design, the degrees of freedom of the design are usually reduced by defining some fixed parameters, such as stacking, preliminary camber [1], wedge angles, blade metal angles, leading and trailing edge radii or thicknesses, lean angle and stagger [8].

The parameters or control points are then manipulated by the optimizer, which will then assess the design against some specified objective function, by processing the flow data output

from the flow solver. Many commercial and in-house CFD codes have been implemented in different design strategies, and they will not be discussed here, except to mention that most commonly Navier-Stokes solvers are chosen to increase precision of the objective function, but a “design mode” or coarser meshing is needed for the iteration, and more precise analysis is left at the last design stage.
The optimization algorithms must be able to seek for the global maximum in multi-dimensional, multi-modal, non-linear and discontinuous design spaces, avoiding local maxima or noise. Evolutionary algorithms (EA) have been the most popular, thanks to their robustness and theoretical simplicity. Examples include evolutionary strategy (ES) [1,7], genetic algorithm (GA) [3,6], multi-objective genetic algorithm (MOGA) [1-2-9] and multiploid MOGA (MOGAXL) [8]. Also adaptive simulated annealing (ASA) [6] has been found to be effective. An alternative approach has also been developed based on the Design of Experiments Method coupled with surrogate models such as Response Surface [10] or neural network (NN) based algorithms [11].

Generally speaking, balance between efficiency and effectiveness of the optimization strategy involves a compromise between flow solver accuracy, number of parameters describing the geometry and computational cost of the optimizer.

In the present study, inverse design software was coupled to an optimizer; a similar strategy applied to pump impellers can be found in the papers of Zangeneh et al. [9,12]. The inverse design software computes the blade shape for a specified distribution of blade loading and also provides a 3D inviscid flow prediction through the designed blade passage. By using the blade loading parameters, it is possible to cover a large part of the design space with a few design parameters. Furthermore, the inverse design code provides an accurate 3D inviscid flow field which can be used to relate to major sources of loss in the rotor. In this way the need to use computationally expensive Navier-Stokes (NS) solutions during the optimization process can be avoided. The advantages are the ability to represent a very broad design space with few variables, the rapid flow evaluation and a more direct control over aerodynamic performance (pressure distribution and work output are directly controlled). However, there is not much control over the geometrical constraints for structural integrity or manufacturability, and viscous or boundary layer effects and associated losses are not included in the design iteration.

A solution is proposed in this paper, where a high-efficiency LP turbine blade showing FEA stress levels above allowable is optimized reducing stresses considerably while maintaining peak efficiency.
This involved quick estimates of aerodynamic losses from inviscid data, and evaluation of stress levels from 3D geometry features. The possibility of running an optimization in a few hours allowed the experimentation of several combinations of objective functions and constraints, giving an insight on the relationship between geometrical features of the blade and mechanical behaviour, until the best strategy for the current design target was found.

METHOD

Inverse design and blade shape generation

Turbodesign-1 (TD1) is a 3D inviscid inverse design software capable of generating a blade shape according to the specified spanwise swirl $r\bar{V}_\theta$ at leading and trailing edge and streamwise loading $(\partial r\bar{V}_\theta/\partial m)$ at different spanwise locations. This is the key input in inverse design. The spanwise distribution of $r\bar{V}_\theta$ is specified at leading and trailing edge to satisfy the required turbine stage enthalpy drop. The meridional derivative $(\partial r\bar{V}_\theta/\partial m)$ is specified by using the so-called 3-segment approach consisting of a linear central portion linked to LE and TE by parabolic curves (see figure 1). This can be specified at different spanwise locations. The value of $\partial r\bar{V}_\theta/\partial m$ at the hub can be

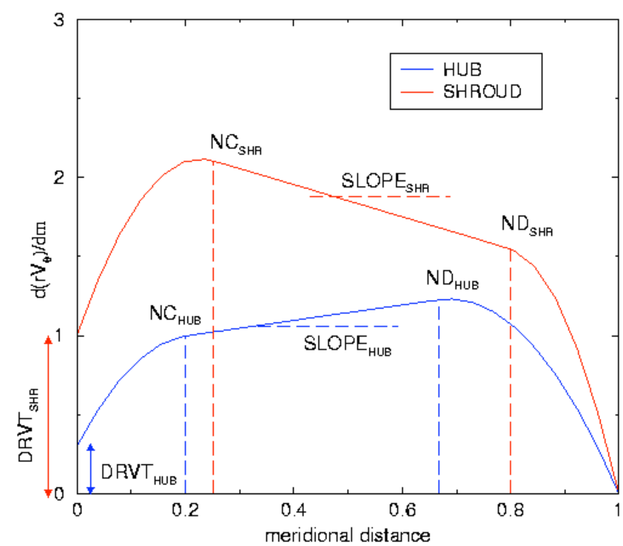

Figure 1: Standard shape for the meridional swirl velocity derivative, with control variables shown.

set to zero to obtain zero incidence or a positive or negative value can be specified to obtain a positive or negative incidence. The value of $(\partial r\bar{V}_\theta/\partial m)$ is set to be always zero at the trailing edge in order to satisfy the Kutta condition. Typically two or three spanwise locations are enough to cover a wide part of the design space. The distribution at each spanwise location is then defined in terms of the parameters DRVT, NC (meridional location for end of first parabolic section), ND (meridional location for start of second parabolic section) and SLOPE (slope of the straight line section). All the blade loading information can be stored in a TD1-dedicated input file (*.pcf file).
The blade geometry is then computed according to the specifications, and inviscid flow data are output which can be

used for the evaluation of objectives and constraints in the optimizer. In order to validate the flow data produced by Turbodesign1, these were compared with results from the commercial CFD code CFX. Figure 2 compares the midspan blade surface pressure distribution for the redesigned blade between Turbodesign1 and CFD stage computations by the commercial CFD code CFX. The agreement is generally good apart from small regions near leading and trailing edges. Hence the surface pressure and Mach number data from Turbodesign1 can be used to help evaluate some of the important aerodynamic performance parameters. This process will be explained in the next section.

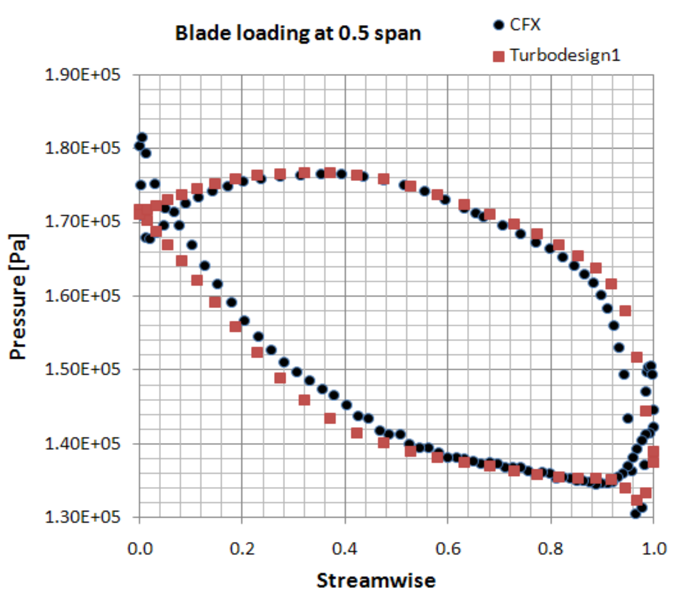

Figure 2: Comparison between inviscid (Turbodesign1) and viscous (CFX) CFD pressure distributions at midspan, for the redesigned blade.

Non-Dominated Sorting Genetic Algorithm

Genetic algorithms are search algorithms based on the mechanics of natural selection and genetics [13] and they operate through a directed-stochastic search technique which can find the optimum solution in complex multi-dimensional search spaces [14].

GAs offer a balance between efficiency and efficacy in the selection process that make them a valid and robust technique for optimization. Also, GAs are not fundamentally limited by restrictive assumptions about the search space (such as continuity, existence of derivatives and unimodality).The robustness of GAs is sustained by the fact that a genetic algorithm [13] follows probabilistic and not deterministic rules; Uses objective function information and not derivatives or other auxiliary information; Works with a coding of the parameters, not with parameters themselves. Although randomized, they exploit historical information to guide the evolution of optimum solutions. It is computationally simple but very effective.

Non-dominated Sorting GA's (NSGA) are particularly suited to multi-objective optimization, as in the present case. In the search space of a multi-objective optimization a set of solutions known as *Pareto-optimal* or *Nondominated* solutions can be found to be superior to all other solutions when all objectives are considered, but inferior when considering individual objectives [15]. Any nondominated solution could be the appropriate design choice since they all satisfy the combination of objectives to the same extent. The final selection has to be performed according to other qualities of the solutions relating to the design outcomes.

Analysis of original stage

The generic aircraft LP turbine rotor to be optimized was generated through Turbodesign1 from the blade loading adapted from a real commercial application; details of the rotor are listed in table 1, while the TD1 blade loading is shown in figure 3.

Rotor Specifications	
No. of Blades	59
Blade mean speed U [m/s]	381
Blade mean height [mm]	56.5
Estimated power [kW]	Ca. 345
Total Enthalpy drop [J/kg]	89557

Table 1: Original aircraft turbine rotor specifications

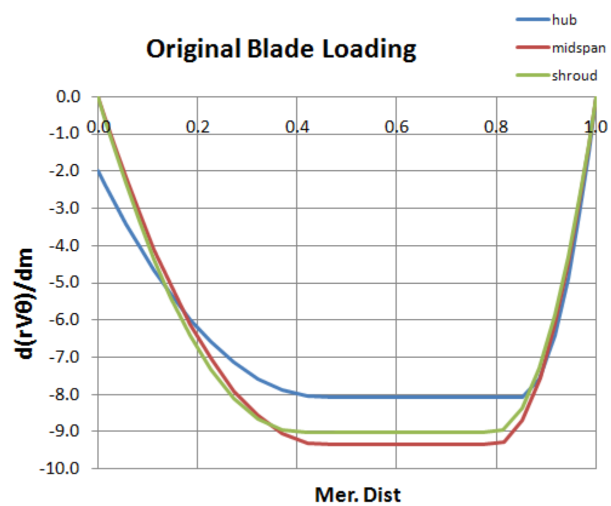

Figure 3: Blade loading used in Turbodesign1 for original rotor blade

The rotor had a nozzle geometry associated with it, allowing the flow through the complete stage to be analysed by means of a RANS solver. The mass, momentum (RANS) and continuity equations together with turbulence eddy dissipation and kinetic energy models were solved with a high-resolution scheme,

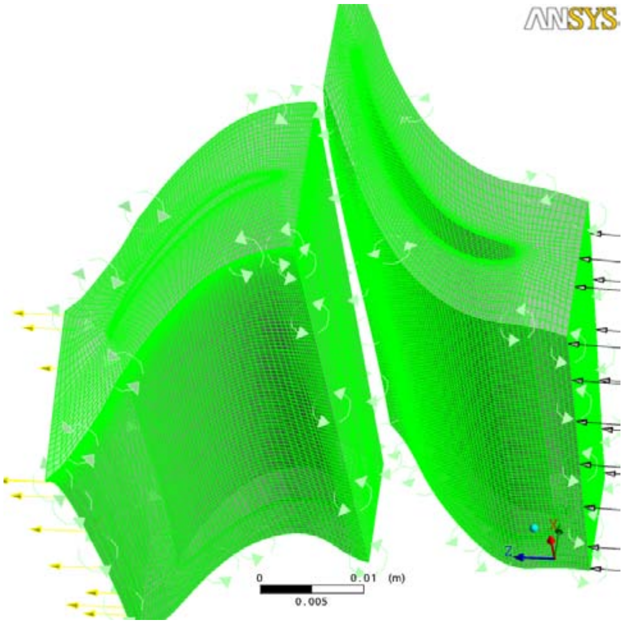

Figure 4: Mesh used for the CFX stage simulation.

using meshes with mixed H-J topology and an O-grid around the blade surface, giving a total of about 250k nodes each for stator and rotor. A tip clearance of 0.5 mm was included for the rotor, and a special mixing-plane interface was used to connect the stationary and rotating domains. Boundary conditions imposed were on stator inlet total pressure of 208638Pa and total temperature 1063K, and outlet static pressure specified according to the mass flow rate required. An outlet static pressure boundary condition was found to be more stable than an outlet mass flow condition, for the CFD code employed in this case. The stage showed already a very high stage efficiency of about 93.3%. A static structural FEA was performed on the rotor blade having angular velocity of 2200rad/sec, and with mechanical properties of Nimonic-115® alloy at about 800^{o}C (E=170GPa, ρ=7850 kg/m^{3,} σ_y=750MPa). The mesh employed for the simulation is shown in figure 15, and has 23017 nodes and 4440 elements. This showed stress levels above yield (figure 13 in annex). The FEA model uses a simple cantilever arrangement for the hub and did not include the proper design of the root and the appropriate fillet radius. As a result the peak stress of 2.39GPa displayed in figure 13 is occurring at the blade root. This is because of a stress concentration present in the computational geometry of the hub support, but it will be eliminated by introducing the actual blade support, properly designed and filleted. The actual stress area of concern was the one at the trailing edge near the hub. It showed the greatest values of equivalent stress, averaging 1.382GPa (ignoring the stress concentration, the area in figure 13 where the probes are located is taken for consideration).

Therefore the main aim of the optimization was to improve mechanical behaviour while maintaining aerodynamic performance, with peak efficiency occurring at the same mass flow rate.

OTPIMIZATION TEST CASE

Design variables and objectives

The optimization tool (NSGA-II, an evolution of NSGA, with more efficient sorting and elitism) in Isight3.0 was coupled to Turbodesign1 and to an in-house post-processing program capable of evaluating some performance parameters, using as input the Turbodesign1 flow field and geometry output.

The loading curve of figure 1 is represented by 4 parameters: NC, ND, central slope and LE loading. The optimizer manipulated these parameters for the hub, midspan and shroud loading; plus two coefficients by which the thickness distribution was multiplied at hub and shroud respectively; the effects of these multiplication factors on the thickness distribution is shown in figure 5.

Therefore, a broad design space was represented with only 14 design variables: these are shown in table 2 with the ranges of variation employed.

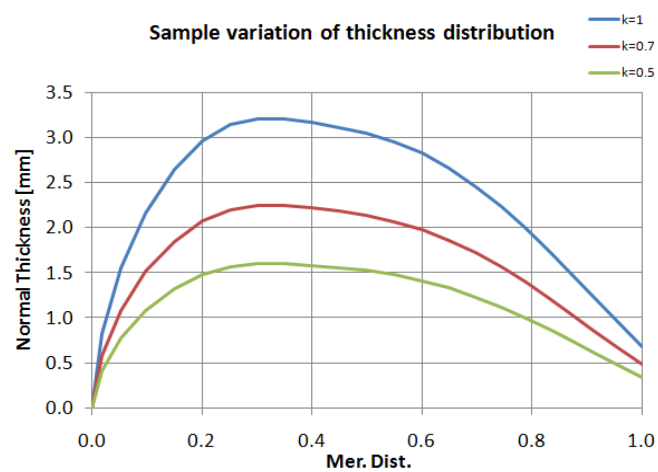

Figure 5: Effects of thickness coefficient variation on the hub thickness distribution

Parameter	Lower Bound	Upper Bound	Parameter	Lower Bound	Upper Bound
LE loading 1	-4.00	0.00	ND 1	0.61	0.95
LE loading 2	-2.00	0.10	ND 2	0.61	0.95
LE loading 3	-2.00	0.10	ND 3	0.61	0.95
NC 1	0.10	0.60	Slope 1	-0.50	0.50
NC 2	0.10	0.60	Slope 2	-0.50	0.50
NC 3	0.10	0.65	Slope 3	-0.50	0.50
Th hub	0.60	1.10	Th shroud	0.55	0.60

Table 2: Design variables and respective ranges of variation

The objective functions chosen in order to optimize stress performance of the blade were *blade lean* and a simple stress factor given by $s = d_{max}/I$, estimated at the hub, where d *is* distance from airfoil meridional neutral axis of points on the profile, and I is second moment of area about the (meridional) neutral axis, and d_{max} is the maximum value of d. This stress factor simply comes from the expression for the extreme fibre stress $\sigma_x = \frac{M}{I} d_{max}$, but avoids including the evaluation of the bending moment at each span location, which is computationally expensive in the context of iterative optimization. The underlying assumption was that the greatest magnitude of bending moment was occurring at sections near the hub, hence the computation was restricted to this area. The computation of the neutral axis shown in figure 6 was found from the assumption that this is approximately parallel to the line joining LE and TE points.

Figure 6: Distance d of a point on the profile from airfoil meridional neutral axis

Note that the greatest source of stress in blades is due to misalignment between centrifugal force and radial geometry, giving the tendency of curved or leaned blades to “unwrap” giving rise to high bending stresses. It was observed during sensitivity analysis that reducing blade lean was generally giving a reduction in stresses, hence the choice of the first objective.

Constraints

Throat area was constrained at ±2% of the original, in order to maintain a similar efficiency characteristic with peak occurring at the same mass flow rate. Another geometrical constraint was imposed on the airfoil cross-sectional area near the hub: this prevented an unwanted increase in blade volume (hence mass and centrifugal force) as a response to the minimization of stress factor. In order to maintain the aerodynamic performance of the original blade while structural modifications were taking place, the computation of some meaningful parameters describing aerodynamic behaviour was introduced in the post-processing code. This was done through some correlations relating inviscid flow field and flow properties. Furthermore, after several tests were performed in order to assess the efficacy of the various parameters, it was deemed possible to constrain them at values below the original ones: this implied also a possible improvement in aerodynamic performance.

The three main sources of loss on a LP turbine blade are the profile losses, endwall loss and the tip clearance loss. All of these losses can be related to blade surface velocity. In fact Denton (1993) has given an expression for profile losses which relate the profile loss to the integral of the cube of velocity along the blade surface. Also Denton proposed the following expression given in equation (1) for the entropy generation in the mixing of mainstream and leakage flows:

$$\zeta = \frac{2C_d g c}{\hbar p \cos a_2} \int_0^1 \left(\frac{V_s}{V_2}\right)^3 \left(1 - \frac{V_p}{V_s}\right) \sqrt{\left(1 - \left(\frac{V_p}{V_s}\right)^2\right)} \frac{dz}{C} \qquad [1]$$

Where the tip-leakage discharge coefficient was taken as $C_d = 0.8$ (Denton 1993).The second correlation gives an estimate of entropy generation in end-wall boundary layers. End wall losses are accounted to be 1/3 of the total loss in a turbine stage, and the entropy generation per unit surface area of the endwall is considerably greater than that on blade surfaces (Denton, 1993). The entropy generation related to surface velocity distribution is given by:

$$\dot{s} = 0.25 \int_0^{c_x} \frac{C_{dis}}{T} \frac{V_s^4 - V_p^4}{V_s - V_p} \rho w \, dx \qquad [2]$$

Here the same dissipation coefficient used in boundary layer entropy generation estimates is used, with a value of $C_{dis} = 0.002$ (Denton and Cumpsty, 1987).

Both the integrals could be easily evaluated from the accurate inviscid surface and mean velocity distributions output from TD1 using a numerical integration method, since values of pressure and suction surface velocities are available at different meridional positions.

A low upper constraint was also imposed on *diffusion ratio* (also based on inviscid surface velocity data) defined as the ratio of peak relative Mach number on the suction surface to the exit mean Mach number on the suction surface. Keeping a low value of diffusion ratio reduces the chances of flow separation.

RESULTS AND DISCUSSION

The multi-objective optimization was set up with details shown in table 3 and run for 9 hours on a single Intel Xeon processor to give the Pareto front of figure 7. Out of the solutions on the front, the one picked is approximately shown in figure 7, since it gave the best compromise having low values for both objectives. Values of original and optimized objectives and constraints are displayed in table 4. The new blade loading is shown in figure 8, and comparison between original and optimized blade thickness distributions are shown in figure 9.

NGSA-II	
Population size	15
Number of generations	500
Crossover probability	0.9
Crossover distribution index	10
Mutation distribution index	20
Initialization mode	Random

Table 3: NGSA II optimization settings

A comparison between stress levels in the original and new blade design is shown in figure 13 (annex). Note again that the peak value of stress is computed at the hub trailing edge; this stress concentration arises because of the flat support used in the FEA solver. In real life a fillet will be introduced, while the

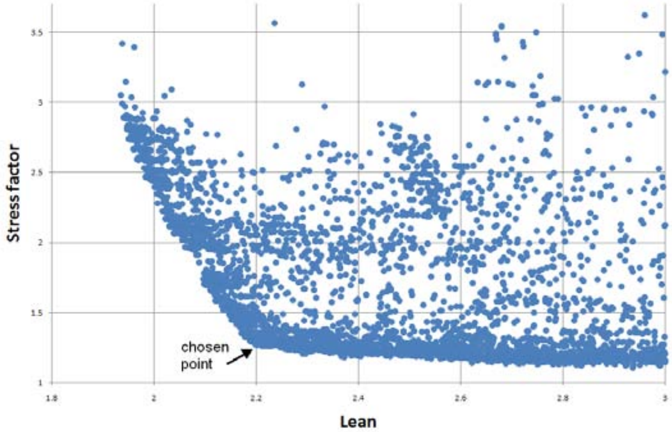

Figure 7: Pareto scatter at the end of the optimization, showing the chosen optimum design

	Original	Optimized	
Mechanical Parameters			**Units**
Max Blade Lean	3.411	2.1834	Degrees
Stress Factor	1.5832	1.2712	1E-09/m³
X-Sectional Area	1.3642	1.3996	mm²
Centrifugal Stress	28.6276	23.5912	1E03*(m/s)²
Aerodynamic Parameters			
Diffusion Ratio	1.1658	1.1268	nd
Tip Leakage Loss	1.1499	1.1102	nd
Endwall Loss	2.2459	2.712	100*kJ/(s*kg*K)
Throat Area	2.016	2.0416	0.01*m²
FEA and CFD Results			
Average Maximum Stress	1.382	0.557	1E9*Pa
Peak Stress	2.51	0.88	1E9*Pa
Peak Efficiency	0.933	0.935	nd
Power Output	284	286	kW

Table 4: Optimization objectives and constraints, for original and optimized blade

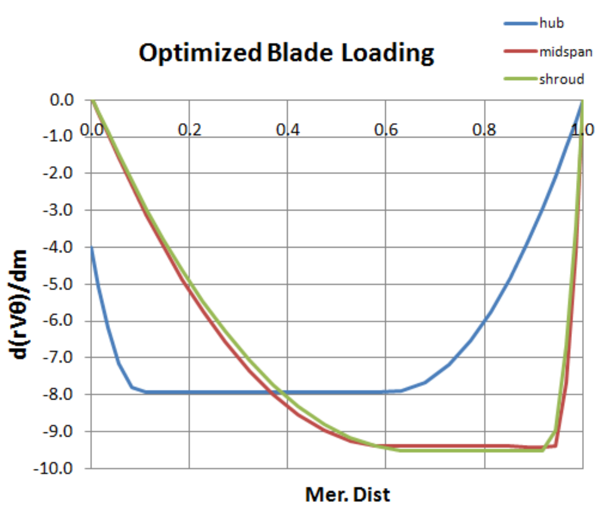

Figure 8: Optimized Turbodesign1 blade loading

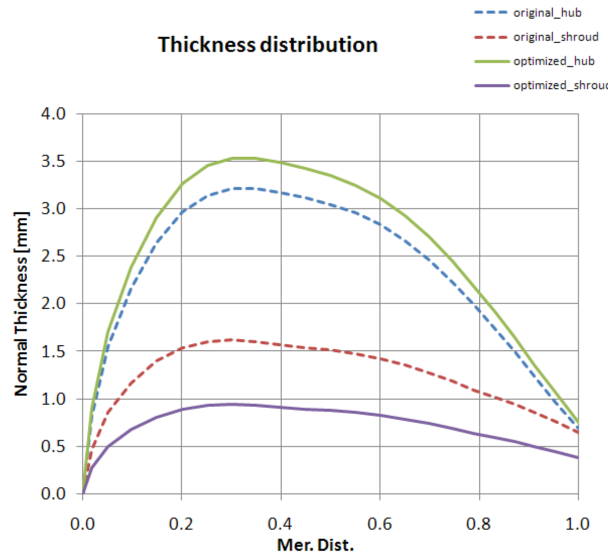

Figure 9: Comparison between original and optimized blade thickness distributions

supporting stress will be distributed on the grooves of the slot-base. This means that even if also the displayed scale shows maximum stress above yield for Nimonic (σ_y=750MPa at 800°C), it is likely to be removed by filleting the base, or introducing the actual base slotted support, and it will be therefore ignored here. The comparison will be between the areas of high equivalent stress in the original and optimized blade (the areas in figures 13 and 14 annex, where probes have been introduced); as a rough estimate the average maximum stress has reduced from 1382MPa to 557MPa, giving a reduction of about 60%, and bringing the stress levels within allowable limits with safety factor 1.35. The maxima in figure 12 show a reduction from 2380 to 830MPa (65%), which means that once the stress concentration is removed, the stress levels at hub also have improved considerably.

To confirm the aerodynamic performance, 8 RANS simulations were run varying stage outlet static pressure, using the same nozzle row employed in the first test. This allowed plotting the efficiency characteristic of figure 12. Note that the peak value of stage efficiency has actually increased from 93.3% to 93.8%: this is not negligible and it suggests that some potential development is available in the aerodynamic design area. It is also very important to note that it occurs at the same mass flow rate as the original one. The stage inlet conditions are the same for both cases.

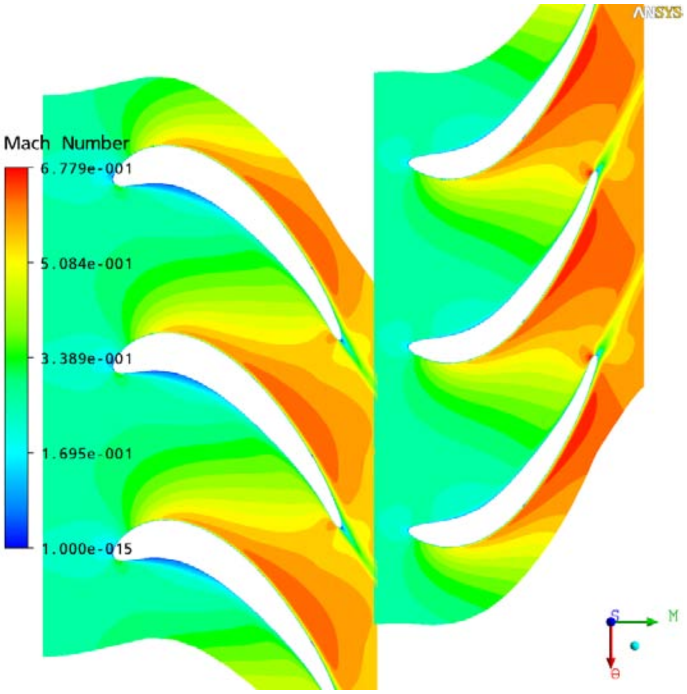

Figure 10: Mach contours at midspan for the stage with redesigned rotor.

The Mach contours at midspan for optimum flow rate are shown in figure 10. Note that no separation occurs on the rotor. Another thing to note is the flow around the nozzle, which shows that some improvements are needed for this component of the stage.
The reduction in stress shown in figure 13 was obtained, as explained earlier, through the simultaneous reduction of blade lean and the newly estimated stress factor. It was shown to what extent these were reduced in value (table 4) and the effect on stress levels has been shown. It is now interesting to observe variations in geometry: figure 11 shows a comparison between original and optimized blade cross sections at different span locations. The blue profile represents the new blade while the white profile is the starting one. The most apparent difference is

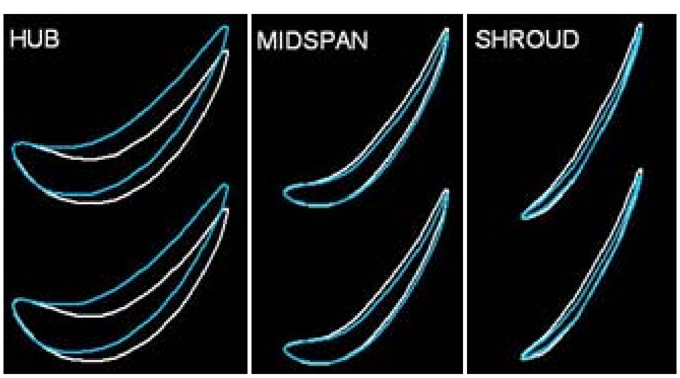

Figure 11: Comparison between sections of original (white) and redesigned (blue) rotor blade

observed at the hub with the new blade showing increased stagger angle, increased thickness and reduced wrap angle. At midspan the two geometries almost match while at shroud the only observable difference is the reduced thickness of the new blade. Having the same stagger and wrap angles at midspan and shroud but reduced wrap angle at hub means that the blade is now more "straight", i.e. the blade is less leaned, with lower level of twist in the stacking. The combination of thickness variation and this distribution of stacking are the features that helped in reducing the stress levels.
Observing the FEA stress distribution and the new hub geometry suggests that variation of thickness factors alone is not an effective way of varying the blade profile, as can be observed by the abundance of material in areas were the bending fibre stress is very low: being able to vary thickness distribution in a similar way to loading distribution could make a more efficient method of optimizing the geometry, also because it was observed that the thickness factors employed in the current optimization tend to converge towards the minimum range value at shroud and maximum at hub. This could come together with improvements in aerodynamic design, perhaps with the addition of other correlations to include blade surface losses and wake mixing losses.

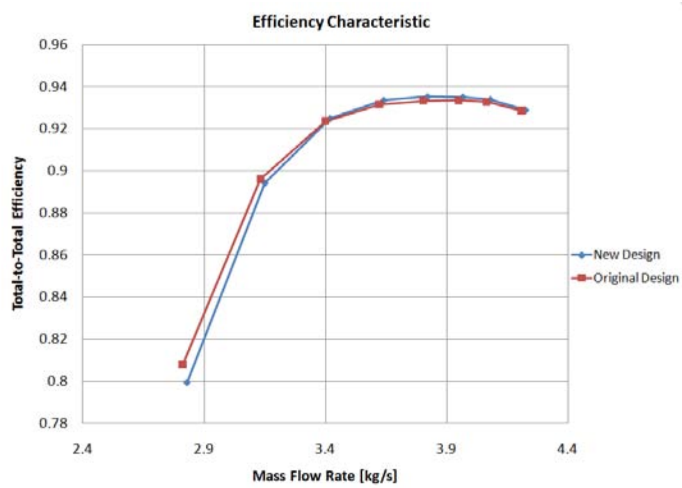

Figure 12: Stage efficiency plot for original ad redesigned rotor blade

CONCLUSION

A methodology for rapid multidisciplinary optimization of turbine blades was presented. The parameterization of blade geometry through blade loading allows the representation of a very broad design space through very few variables; furthermore it gives a more direct control over the aerodynamic performance since specific work and blade pressure distribution depend on the prescribed blade loading. Having few design variables is ideal for optimization through evolutionary algorithms, reducing the exploration time considerably and speeding up convergence. Also, the prompt availability of inviscid flow data from the inverse design method, allows the evaluation of aerodynamic performance parameters through correlations, which is much faster than the classic introduction of a CFD solver in the optimizer loop. Similarly, simple stress estimates from geometrical considerations take a fraction of a second in the optimizer, and their effectiveness can be readily tested with a FEA tool once the optimized geometry is produced.

An additional advantage of having a rapid optimization method (rather than a more accurate but considerably more lengthy one) is the possibility to test several optimizer configurations, until the best combination of design variables, constraints and objectives is found to represent design quality at its best.

The effectiveness of this method was proved with the test case in this paper, where a highly stressed LP turbine blade was optimized with a 9hr automatic optimization, improving structural performance considerably while maintaining consistent efficiency characteristic and a 0.5% increase in peak stage efficiency.

REFERENCES

[1] Sonoda, T., et al., 2004, “Advanced High Turning Compressor Airfoils for Low Reynolds Number Condition— Part I: Design and Optimization”, ASME Journal of Turbomachinery, Vol. 126, pp. 350-359

[2] Sonoda, T., et al., 2006, “A Study of Advanced High-Loaded Transonic Turbine Airfoils”, ASME Journal of Turbomachinery, Vol. 128, pp. 650-657

[3] Oyama, A., Liou, M., Obayashy, S., 2002, “ Transonic Axial-flow Blade Shape Optimization using Evolutionary Algorithm and Three-dimensional Navier-Stokes Solver”, AIAA paper 2002-5642

[4] Dennis, B. H., Egorov, I. N., et al., 2000, “Multi-objective Optimization of Turbomachinery Cascades for minimum Loss, Maximum Loading, and maximum Gap-to-chord ratio” , AIAA paper 2000-4876

[5] Kontoleontos, E. A., Giannakoglou, K. C., Koubogiannis, D. G., 2005 “ Robust Design of Compressor Cascade Airfoils, using Evolutionary Algorithms and Surrogate Models”, 1st International Conference on Experiments/Process/ System Modelling/Simulation/Optimization, 1st IC-EpsMsO, Athens 6-9 July, 2005

[6] Chen, B., and Yuan, X., 2008, “Advanced Aerodynamic Optimization System for Turbomachinery”, ASME Journal of Turbomachinery, Vol. 130, Issue 2.

[7] Hasenjager, M., Sendhoff, B., Sonoda, T., Arida, T., 2005, “Three dimensional aerodynamic Optimization for an Ultra-low Aspect Ratio transonic Turbine Stator Blade” ASME paper GT2005-68680

[8] Oksuz, O., Akmandor, I. S., 2010, “Multi-Objective Aerodynamic Optimization of Axial Turbine Blades Using a Novel Multilevel Genetic Algorithm”, ASME Journal of Turbomachinery, Vol. 132, 041009

[9] Zangeneh, M., DaCosta, B., and Dakeshkahna, K., 2008, “Multi-Objective Automatic Optimization Strategy for Design of Waterjet Pumps”, RINA Waterjet Propulsion Conference, London.

[10] Bonaiuti, D., and Zangeneh, M., 2009, “On the coupling of inverse design and optimization techniques for multi-objective, multi-point optimization of turbomachinery blades”, ASME J. of Turbomachinery, Vol. 131, 021014.

[11] Papila, N., Shyy, W., Griffin, L., Dorney, D. J., “Shape Optimization of Supersonic Turbines Using Global Approximation Methods”, Journal of Propulsion and Power, Vol. 18, No. 3, pp 509-518

[12] Zangeneh, M., Daneshkhah, K., 2009, ‘A fast 3D inverse design based multi-objective optimization strategy for design of pumps’ ASME Paper FEDSM2009-78443.

[13] Goldberg, D.E., 1989, Genetic Algorithms in search, optimization and machine learning, Addison-Wesley, Boston.

[14] Pham, D.T., and Karaboga, D., 1998, Intelligent Optimisation Techniques, Springer, London.

[15] Srinivas, N., and Deb, K., 1994, “Multiobjective Optimization using Nondominated Sorting in Genetic Algorithms”, Evolutionary Computation, Vol. 2, pp. 221-248.

[16] Denton, J.D., 1993, “Loss Mechanisms in Turbomachines”, ASME Journal of Turbomachinery, Vol. 115, pp. 621-656.

[17] Denton, J.D., and Cumpsty, N.A., 1987, “Loss Mechanisms in Turbomachines”, IMechE Paper No. C260/87.

[18] Chankong, V., and Haimes, Y. Y., 1983, Multiobjective Decision Making Theory and Methodology, North-Holland, New York

ANNEX

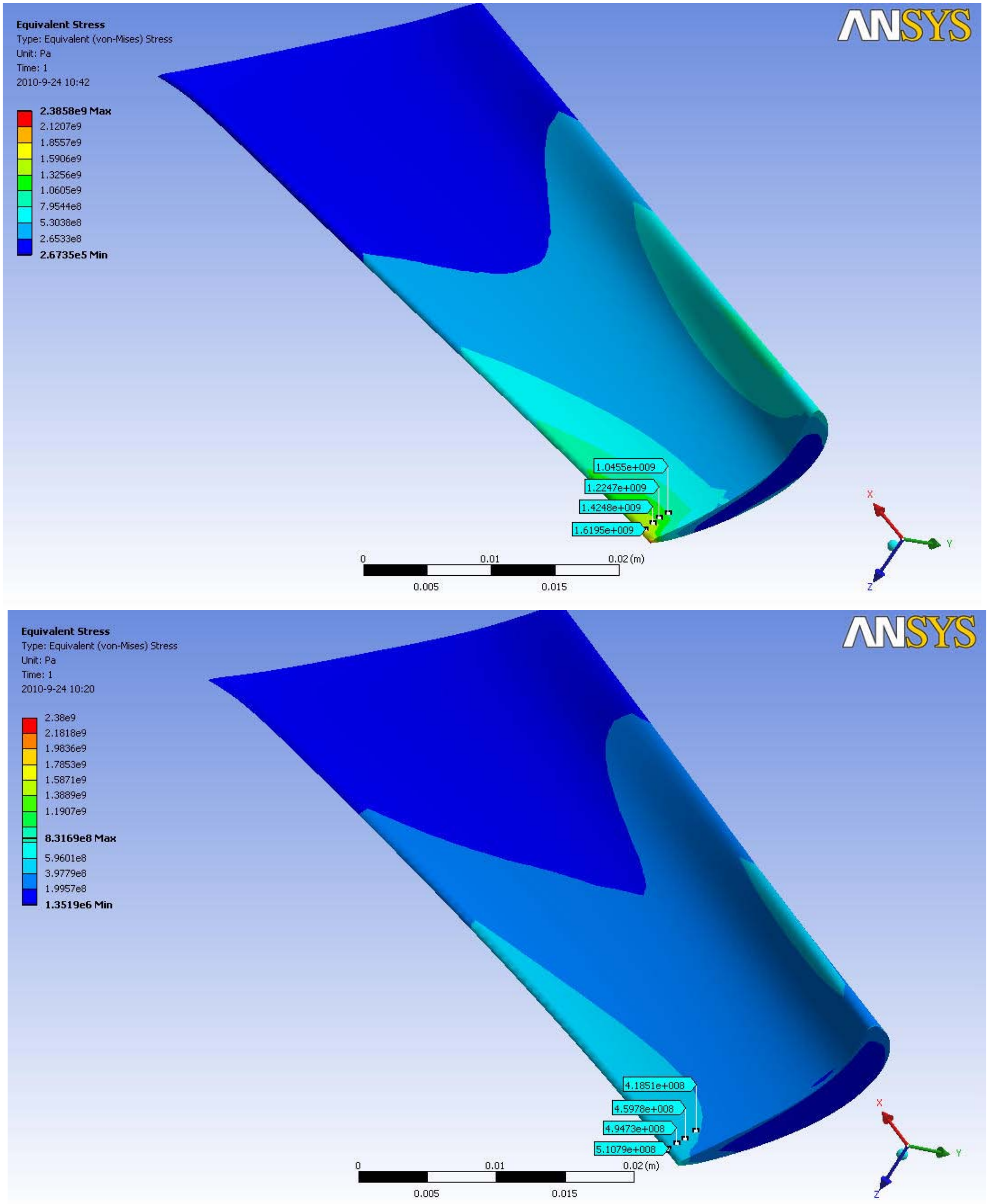

Figure 13: Comparison between original (top) and optimized (bottom) stress levels under centrifugal forces

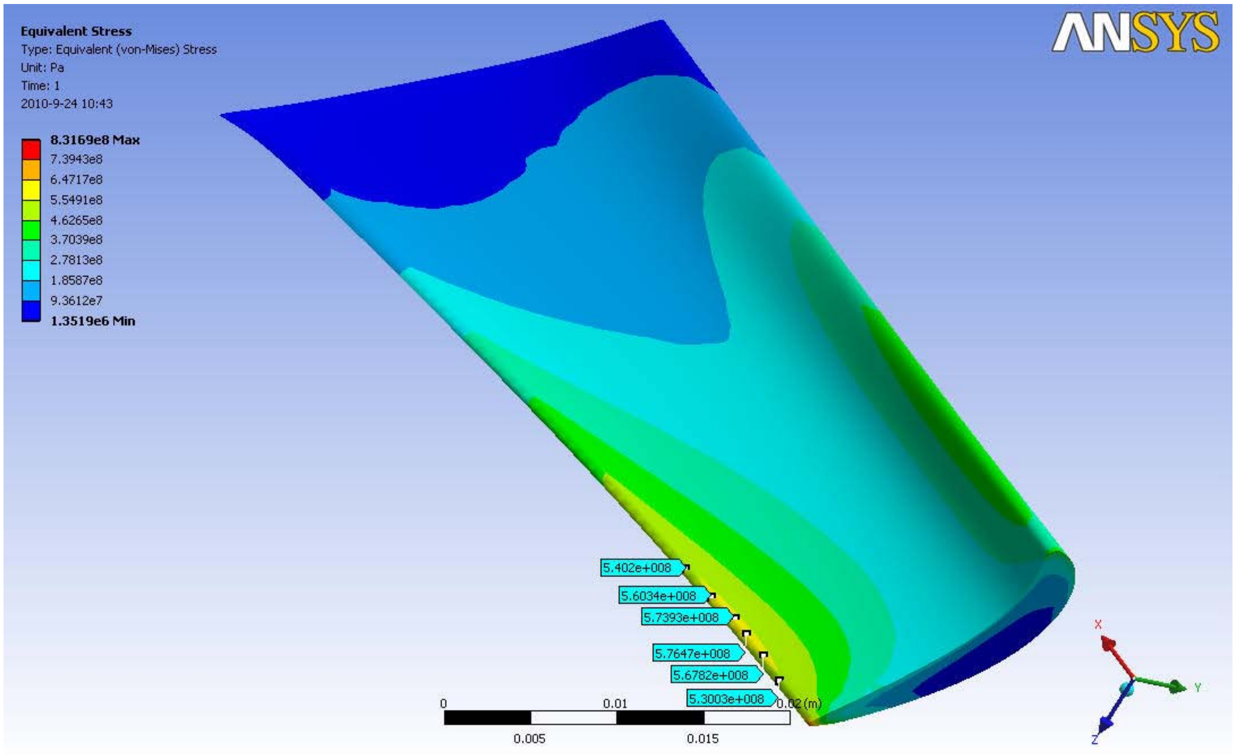

Figure 14: Detail of the redesigned rotor stress levels under centrifugal forces

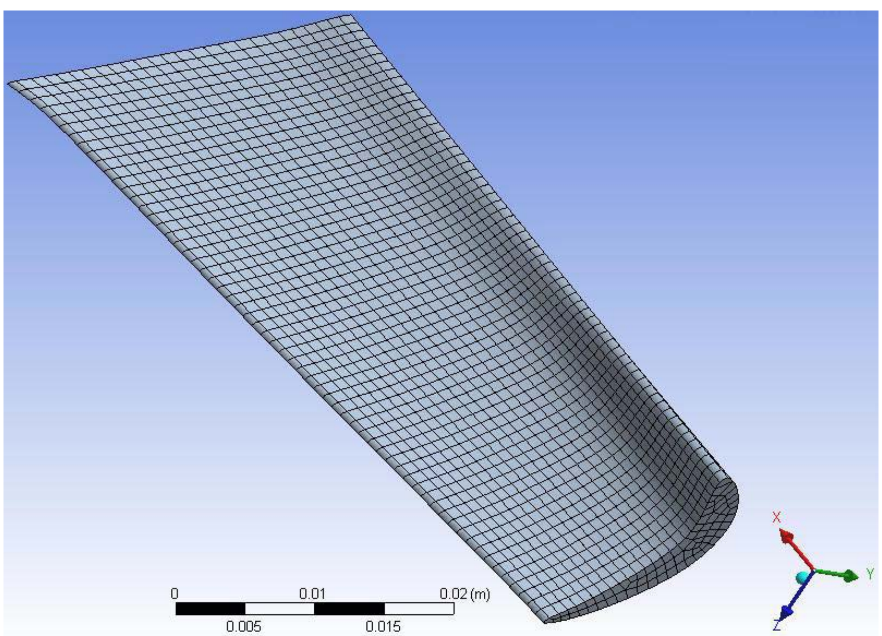

Figure 15: Mesh employed for the FEA on the rotor blade.